X-730-72-323

PREPRINT

NASA TM X- 66046

PROPAGATION OF RADIO WAVES THROUGH THE LOWER ATMOSPHERE OF VENUS

KURT R. RICHTER

AUGUST 1972

GSFC

GODDARD SPACE FLIGHT CENTER

GREENBELT, MARYLAND

X-730-72-323

PROPAGATION OF RADIO WAVES THROUGH THE LOWER ATMOSPHERE OF VENUS

Kurt R. Richter*
Advanced Projects

August 1972

*On leave of absence from the Institut fuer Hochfrequenztechnik of the University of Technology, Vienna, Austria.

GODDARD SPACE FLIGHT CENTER
Greenbelt, Maryland

PROPAGATION OF RADIO WAVES THROUGH THE LOWER ATMOSPHERE OF VENUS

Kurt R. Richter
Advanced Projects

ABSTRACT

A simplified model of the Venus atmosphere is developed providing the loss factor profile of the atmosphere. With this profile the atmospheric attenuation as it depends upon the incidence angle is calculated for wavelengths between 2 cm and 20 cm. It is shown that the signal-to-noise ratios for a real aperture radar, a synthetic aperture radar, and communication links between a satellite and a landing probe achieve maximum values by the proper choice of the wavelengths. Furthermore, it turns out that the wavelength dependence is less crucial for the synthetic aperture radar compared to the other cases.

CONTENTS

ILLUSTRATIONS

PROPAGATION OF RADIO WAVES THROUGH THE LOWER ATMOSPHERE OF VENUS

INTRODUCTION

Knowledge on the atmosphere of Venus has increased rapidly in the last decade. Reasons for this development have been improved measurements of the brightness temperature and radar reflections of the planet. The most important facts, however, have been provided by planetary fly-by experiments of Mariner 2 and 5 and the Venera probe missions.

Results from these experiments confirmed the existence of a dense atmosphere consisting mainly of carbon dioxide at high temperature and pressure at the surface. Furthermore, the results gave insight into the dependence of these parameters upon the altitude above the surface of the planet.

Since this dense atmosphere obscures the planet so well almost nothing is known about its surface features. Only radar mapping in the microwave region seems to be promising to lift this veil as has been shown by earth based radar. However, even near the subearth point the resolution of these radar systems is too low to show detailed pictures of the planet's surface.

There is no doubt that in the future a spacecraft-borne microwave radar orbiting the planet will be used to explore the structure of the surface.

This paper is concerned with the selection of the operating frequencies for different radar systems and for communications from a probe situated on the surface of the planet to a spacecraft, and vice versa. The operating frequency

should provide a maximum signal-to-noise ratio taking into account the constraints in Aerospace Systems on the antenna dimensions, the wavelength dependence of the attenuation in the atmosphere of Venus, and the received noise power radiated from the surface and the atmosphere. For this purpose a simplified model of the atmosphere will be used to calculate the antenna temperatures for different systems.

MODEL OF THE LOWER ATMOSPHERE OF VENUS

In Figure 1 and Figure 2 the temperature and pressure profiles are based on data given by AVDUEVSKY et al. [1971], and FJELDBO et al. [1971]. These profiles represent a simplified model since they are smoothed curves.

Assuming a pure CO_2 atmosphere according to KUZMIN and VETUKHNOVSKAYA [1968] the refractivity profile N(y) may be calculated as

$$N(y) = K_1 \, P(y)/T(y) \tag{1}$$

Where $K_1 = 0.1345°K/atm$, and P(y) and T(y) are pressure and temperature at an altitude y. N(y) is shown in Figure 3.

To obtain the temperature of an antenna looking down from space toward the surface of the planet or looking into the space from the surface the profile of the loss factor $\alpha(y)$ must be known. Based on the results by HO et. al. [1966] and MUHLEMAN [1970], the loss factor per km due to CO can be written as

$$\alpha_{CO_2}(y) = \frac{15.7 \cdot 10^{-3}}{\lambda^2} (273)^5 \cdot P^2(y)/T^5(y) \quad km^{-1} \tag{2}$$

which shows a quadratic increase for decreasing wavelength.

However, the attenuation measured by Mariner 5 at 13 cm wavelength in a region below 52 km altitude above the surface can not be explained by a pure CO_2-atmosphere. RICHTER [1972] has shown that the nearly constant loss of 3.5 dB/km between 52 km and the superrefractive layer at 35 km measured by Mariner 5 may originate from a two-component layer in this altitude range.

Assuming this layer consists of water droplets and water vapor, the losses basically show the same wavelength dependence as $\alpha_{CO_2}(y)$ does. The resulting total loss factor $\alpha(y)$ may then be written as

$$\alpha(y) = \beta(y)/\lambda^2 \tag{3}$$

where the factor $\beta(y)$ is independent upon the wavelength.

In Figure 4, the simplified model for exp $[\beta(y)]$ is shown. The dashed line represents the losses due to CO_2 only, and the dots indicate the losses measured by Mariner 5.

According to the Mariner 5 measurements the simplified model uses a constant loss factor of $0.59/\lambda^2$ dB/km which is constant between 26 km and 52 km. Above and below this altitude range the losses show the altitude dependence according to (2) assuming that in this part only CO_2 is present. In this model the attenuation above 52 km has been neglected.

Even though it is a rather coarse model for the attenuation in the atmosphere of Venus minor changes of the loss factor profile in the altitude range between 25 km and 52 km have only insignificant influence on the total attenuation of electromagnetic waves propagating through the atmosphere.

PLANAR MODEL

The total attenuation of electromagnetic waves propagating through a lossy medium is dependent upon the path length which, in the case of the spherical model of Venus, is a function of the incidence angle γ_0 of the ray on a certain layer in the atmosphere. In this paper, this reference layer is chosen at 90 km above the surface where the refractive index n ($n(y) = 1 + N(y)\ 10^{-6}$) may be assumed to be unity (see Figure 5).

Radio waves in such an atmosphere propagate like light waves in a spherical glass lens with radially varying refractive index n(y). Therefore, Snell's law

$$r \cdot n(r) \sin \gamma(r) = \text{const.}$$

is applicable, where n(r) is the refractive index of a spherical layer of the lens with the radius r at which the incidence angle is $\gamma(r)$. According to our model it is

$$(R_0 + y)\ n\ (y) \sin \gamma(y) = (R_0 + 90) \sin \gamma_0 . \qquad (4)$$

Here $R_0 = 6050$ km (radius of the planet), y is the altitude above the surface in km, and $\gamma(y)$ and γ_0 are the incidence angles at y and 90 km altitude, respectively. However, it can be shown from (4) that for $\gamma_0 \leq 70°$ the variation of γ (y) is so small that the spherical model can be dropped and a planar model can be assumed. In this case, the incremental ray path length ds is

$$ds = dy/\cos \gamma_0 . \qquad (5)$$

Integration from the surface up to 90 km altitude for $\gamma_0 = 70°$ yields a deviation less than 2% between the total path lengths of the planar and the spherical model, respectively. This error increases rapidly for $\gamma_0 > 70°$ and becomes infinite for $\gamma_0 \approx 83°$. At this incidence angle the ray is trapped in the superrefractive layer ($y \approx 35$ km) and the spherical model theoretically yields an infinitely long ray while integration of (5) still results in a finite ray length. However, for the purposes of radar mapping and communication, incidence angles larger than 70° are of little interest. Therefore, in all further investigations, the planar model and incidence angles $\gamma_0 \leq 70$ will be considered.

ATMOSPHERIC ATTENUATION

An electromagnetic wave propagating through an atmosphere according to the developed planar model (incidence angle γ_0) is attenuated at the surface of the planet by 1/L where

$$1/L = \exp\left[-\int_0^{\ell} \alpha(y)\, dy/\cos\gamma_0\right] \quad . \tag{6}$$

The upper limit, ℓ, of the integral can be taken as 52 km because in the particular model of the atmosphere there is no attenuation above an altitude of 52 km. According to (3) the one way attenuation 1/L may be written as

$$1/L = \exp\left[-\frac{\int_0^{\ell} \beta(y)\, dy}{\lambda^2 \cos\gamma_0}\right] = \exp\left[-\frac{M}{\lambda^2 \cos\gamma_0}\right] , \tag{7}$$

where

$$M = \int_0^{\ell} \beta(y)\, dy \quad . \tag{8}$$

Evaluating the integral in (8) yields $M = 17.32$ cm^2 so that the opacity or optical thickness $\tau(\lambda, \gamma_0)$ (which is the positive exponent in (7)) is written as

$$\tau(\lambda, \gamma_0) = \frac{17.32}{\lambda^2 \cos \gamma_0} \quad . \tag{9}$$

The opacity calculated here is about 20% higher than the value calculated by MUHLEMAN [1970] according to the higher pressure and temperature at the surface and to the additional attenuation in the altitude range between 25 and 52 km.

In Figure 6 and Figure 7, the normalized one-way attenuation and the normalized opacity respectively are shown. In order to obtain the attenuation and/or opacity at a certain wavelength, the respective values from the figures must be divided by λ^2 (λ in centimeter).

ANTENNA TEMPERATURE

The temperature of a receiving antenna from outside of the atmosphere directed toward the surface of the planet can be calculated according to KUZMIN and VETUKHNOVSKAYA [1968] from

$$T_{a\downarrow} = \epsilon\, T_0 \exp\left[-\frac{M}{\lambda^2 \cos \gamma_0}\right] + \int_0^{52} T(y)\, \frac{\beta(y)}{\lambda^2 \cos \gamma_0} \exp\left[-\frac{\int_y^{52} \beta(t)\, dt}{\lambda^2 \cos \gamma_0}\right] dy$$

$$+ (1-\epsilon) \int_0^{52} T(y)\, \frac{\beta(y)}{\lambda^2 \cos \gamma_0} \exp\left[\frac{\int_y^{52} \beta(t)\, dt - 2M}{\lambda^2 \cos \gamma_0}\right] dy \tag{10}$$

where ϵ is the emissivity of the surface and T_0 is the surface temperature of the planet. All other terms have been defined before.

On the right hand side of (10), the first term represents the temperature according to the noise received from the surface the second term the noise directly received from the atmosphere and the last term the atmospheric radiation as reflected from the surface.

For an assumed emissivity of 0.9, the antenna temperature $T_{a\downarrow}$ was calculated by numerical integration for different wavelengths in the range between 2 cm and 20 cm. The resulting antenna temperatures are shown in Figure 8 as functions of the incidence angle γ_0.

A receiving antenna situated on the surface of the planet looking upward receives only the noise power radiated downward by the atmosphere. The corresponding antenna temperature is

$$T_{a\uparrow} = \int_0^{52} \frac{T(y)\,\beta\,(y)}{\lambda^2 \cos\gamma_0} \exp\left[- \frac{\int_0^y \beta\,(t)\,dt}{\lambda^2 \cos\gamma_0} \right] dy \qquad (11)$$

The numerical results are shown in Figure 9.

It must be noted, however, that the antenna is assumed to have no sidelobes pointing toward the surface and the elevation angle is not less than 20°, which would result in a significant increase of the antenna temperature. This means ideal antennas providing very narrow beams (pencil beams) are considered. Due to these assumptions defocusing effects of the atmosphere have been neglected.

C

SIGNAL-TO-NOISE RATIO

Since the antenna temperatures for downlooking or uplooking antennas are now known, the received noise power P_n in terms of a system noise temperature T_s can be expressed as

$$P_n = k T_{s1} B_n \tag{12a}$$

for a downlooking and as

$$P_n = k T_{s2} B_n \tag{12b}$$

for an uplooking antenna, where k is Boltzmann's constant and B_n is the noise bandwidth of the predetection filter. The system noise temperatures are

$$T_{s1} = T_{a\downarrow} + T_R (F_n - 1) \tag{13a}$$

$$T_{s2} = T_{a\uparrow} + T_R (F_n - 1) \tag{13b}$$

where $T_R = 290°K$ is the standard reference temperature and F_n is the noise factor. It can be easily seen that for large noise factors, changes of the antenna noise temperatures are of minor influence.

In aerospace systems, however, there exist weight and dimension limitations so that a certain effective antenna area A may not be exceeded. For this area A the antenna gain decreases by λ^2. On the other hand the attenuation of the signal increases at shorter wavelengths so one can expect the existence of a frequency where the signal-to-noise ratio becomes a maximum.

In the following, three modes of operation will be considered; namely, a real aperture radar, a synthetic aperture radar, and a communication system

between a probe at the surface and an orbiting spacecraft or an earth based station (uplink) and/or vice versa (downlink).

Case 1: Real Aperture Radar

The signal-to-noise ratio (S/N) of a pulse radar system may be written as

$$S/N = \frac{P_t A_t A_r \sigma}{4\pi R^4 k B} \frac{f_1(\gamma_0,\lambda)}{T_{s\downarrow}} \tag{14}$$

where

$$f_1(\gamma_0, \lambda) = \frac{\exp(-2M/\lambda^2 \cos\gamma_0)}{\lambda^2} \tag{15}$$

The numerator of $f_1(\gamma_0, \lambda)$ takes care of the attenuation in the atmosphere, while λ^2 in the denominator originates from the relation between the gain and effective area A of the transmitting antenna. Assuming an wavelength independant term including the achievable transmitter power P_t, the effective areas A_t and A_r of the receiving and transmitting antennas, the noise bandwidth B of the predetection filter, and the radar cross section σ the wavelength dependence of the signal-to-noise ratio is described by the function $f_1(\gamma_0, \lambda)/T_{s\downarrow}$. This function is shown in Figure 10, where the parameter is the incidence angle γ_0. One sees that an altimeter radar ($\gamma_0 = 0$) should be operated at a wavelength $\lambda = 4.75$ cm in order to obtain a maximum S/N. At increasing incidence angles γ_0 the optimum wavelength increases to $\lambda = 10$ cm at $\gamma_0 = 70°$. The units of the ordinate are decibels according to the wavelength given in cm and the system temperature in degrees Kelvin. The values of the system temperature are calculated from (13a) with the antenna temperatures from Figure 8 and assuming a

noise figure F_n = 6 db. Figure 10 also shows the remarkable decrease of the signal-to-noise ratio at larger incidence angles. This decrease is even greater when the angular dependence of the radar cross section σ is taken into account. However, by this fact the shape of the curves would not be influenced, so that the optimum frequencies are still the same.

Case 2: Synthetic Aperture Radar

For a synthetic aperture radar, the radar cross section is dependant upon the wavelength (SKOLNIK [1970]) so that the signal-to-noise ratio results as

$$S/N = \frac{P_{ar}\ A_t A_R \rho \delta_r\ \cos\gamma_0}{8\pi k R^3\ v}\ \frac{f_2(\gamma_0,\lambda)}{T_{s\downarrow}} \quad . \tag{16}$$

Here P_{av} is the average transmitter power, ρ the reflectivity of the surface, δ_r the range resolution, k Boltzmann's constant, R the range, and v the spacecraft velocity. In the wavelength dependent term $f_2(\gamma_0, \lambda)/T_{s\downarrow}$ the system temperature is the same as in case 1 and

$$f_2(\gamma_0, \lambda\ ) = \frac{\exp\ (-2M/\lambda^2 \cos\gamma_0)}{\lambda^2} \quad . \tag{17}$$

In Figure 11 it can be seen that the maximum signal-to-noise ratios occur at longer wavelengths as they did in case 1. Furthermore, the decrease at wavelengths longer than the optimum wavelength is less than it is for a real aperture radar; also the decrease of the maximum due to increasing incidence angles is less significant. This means that the signal-to-noise ratio is much less sensitive to the operating frequency.

Case 3: Communication

Considering the range attenuation, the received signal power S is the same for an uplink and a downlink. Namely,

$$S = \frac{P_t A_t A_r}{R^2} \quad f_3(\gamma_0, \lambda) \tag{18}$$

where

$$f_3(\gamma_0, \lambda) = \frac{\exp(-M/\lambda^2 \cos\gamma_0)}{\lambda^2} \quad . \tag{19}$$

The exponential function takes into account the one-way attenuation in the atmosphere of the planet. The received noise power is calculated from (12a) or (12b) for an uplink or downlink, respectively. In Figure 12 and Figure 13 the wavelength dependent term $f_3(\gamma_0, \lambda)/T_s$ is shown for both cases of communication. It might be noticed that the shift of the optimum frequencies with regard to the incidence angle is rather small compared to the radar cases. However, since the slopes of the curves are very steep the appropriate frequencies are within a narrow band.

CONCLUSION

For three different modes of operation, it has been shown that by a proper choice of the operation frequency the signal-to-noise ratio has a maximum value and decreases rapidly at wavelengths deviating from an optimum wavelength which depends upon the incidence angle γ_0. For a synthetic aperture radar, however, the decrease of the signal-to-noise ratio at longer wavelengths is not significant.

Ignoring the frequency dependence of the background noise, a very good estimate for the optimum frequencies can be achieved from the functions $f_1(\gamma_0, \lambda)$, $f_2(\gamma_0, \lambda)$, and $f_3(\gamma_0, \lambda)$. Optimum wavelengths obtained in this way are shown in Figure 14 as a function of the incidence angle for all three modes of operations.

REFERENCES

Avduevsky, V.S., Marov, M. Ya., Rozhedestvensky, M.K., (1971) Landing of the Automatic Station Venera 7 on the Venus Surface and Preliminary Results of Investigations of the Venus Atmosphere, J. Atmos. Sci., 28, 263-269.

Fjeldbo, G., Kliore, A.J., Eshleman, R., (1971), The Neutral Atmosphere of Venus as Studied with the Mariner V, Astron, J. 76, 123-140.

Ho, W., Kaufman, I.A., and Thaddeus, P., (1966), Laboratory Measurements of Microwave Absorption in Models of the Atmosphere of Venus, J. Geophys. Res., 71, 5091-5108.

Kuzmin, A.D., Vetukhnovskaya, Yu. N., (1968), Venera 4 and Interpretation of Radioastronomical Measurement of Venus, Kosmich, Issled., 6, No. 4, 590-597.

Muhleman, D.O., (1970), Interferometric Investigations of the Atmosphere of Venus, Radio Sc., 5, No. 2, 355-362.

Richter K.R., (1972), Enhanced Microwave Absorption in the Lower Atmosphere of Venus, Radio Sc., 6 No. 4, 443-447.

Skolnik M.I., (1970), Radar Handbook, McGraw-Hill Book Co., Chapter 23.

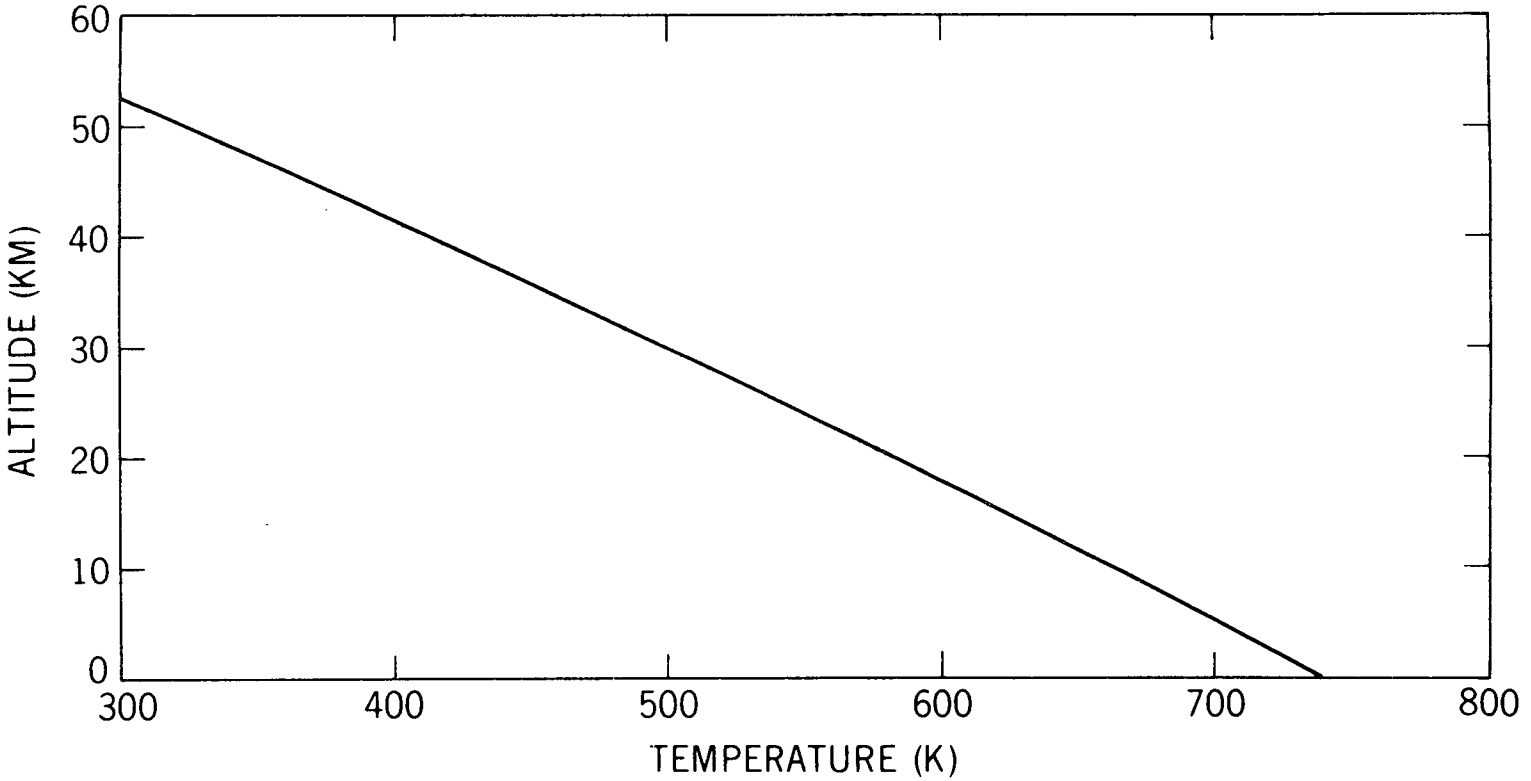

Figure 1. Temperature profile

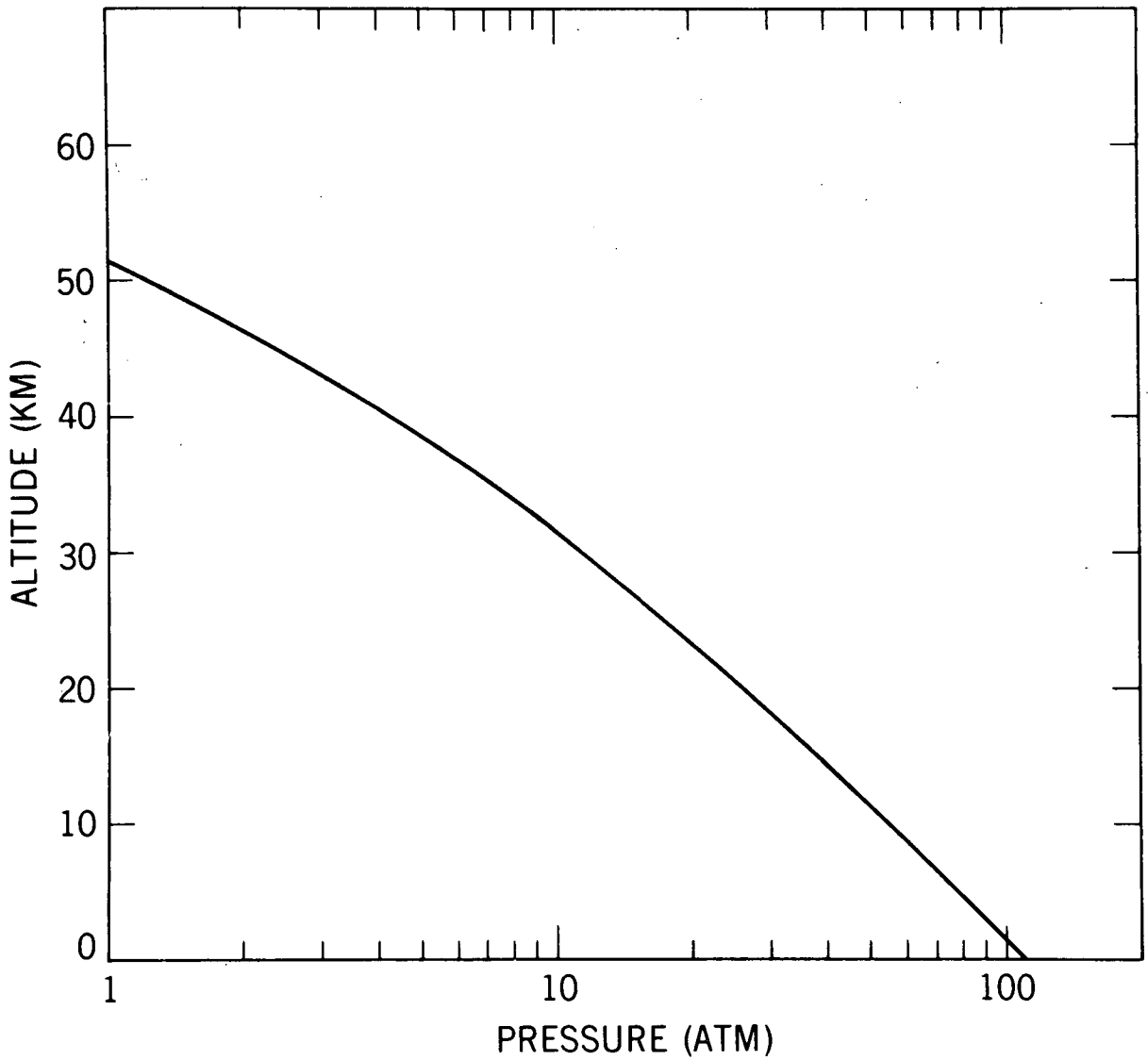

Figure 2. Pressure profile

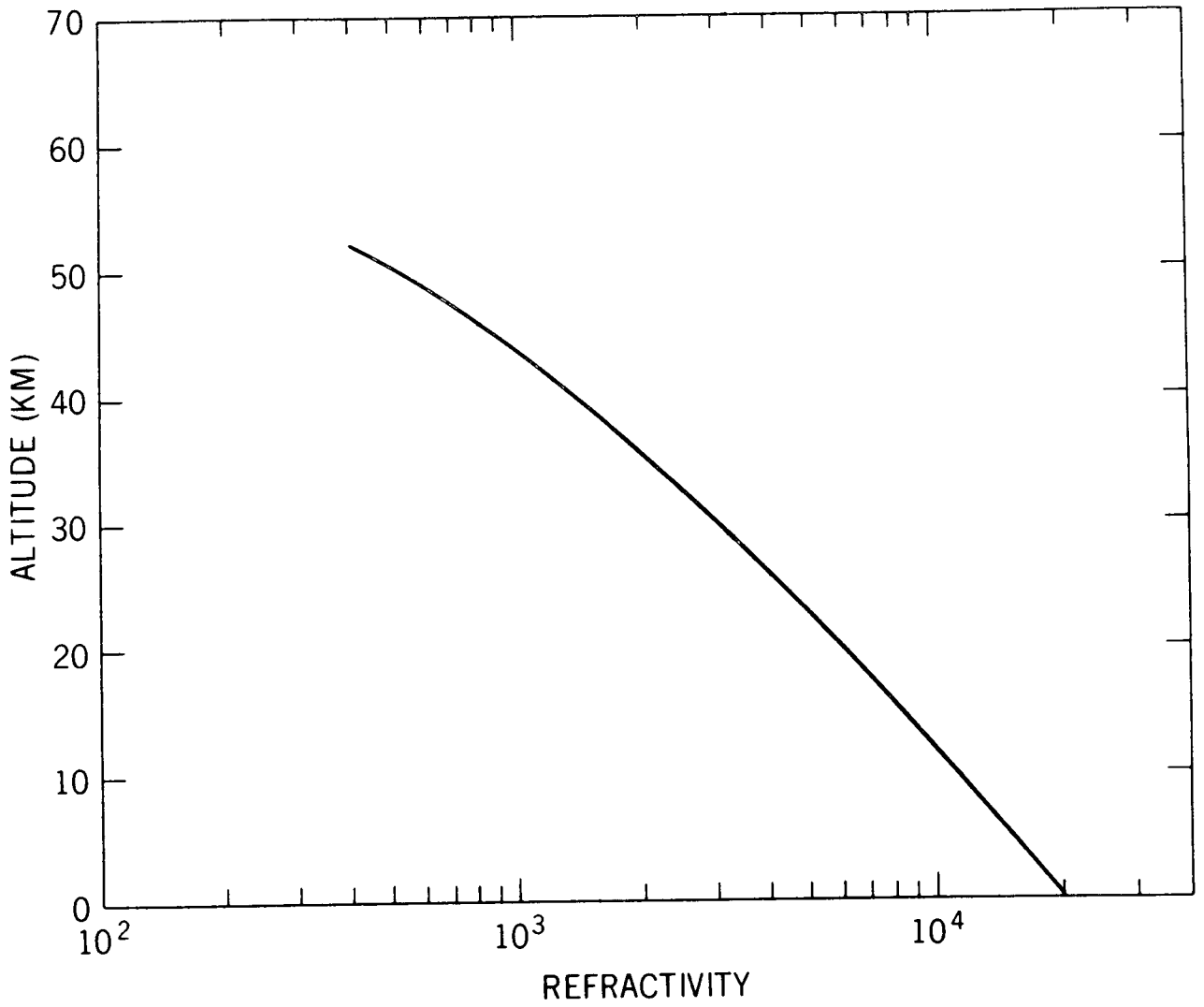

Figure 3. Refractivity profile

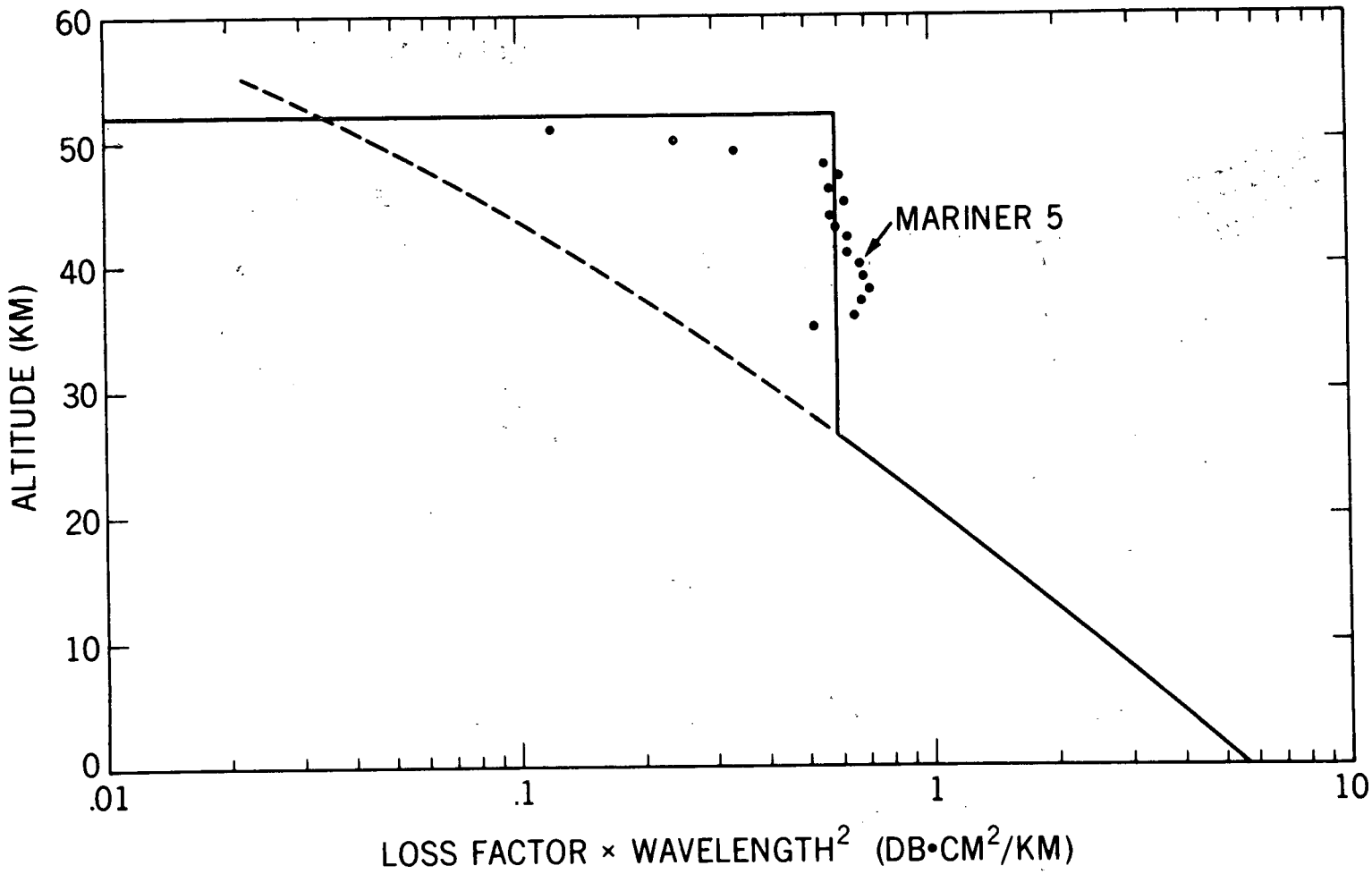

Figure 4. Profile of the normalized loss factor

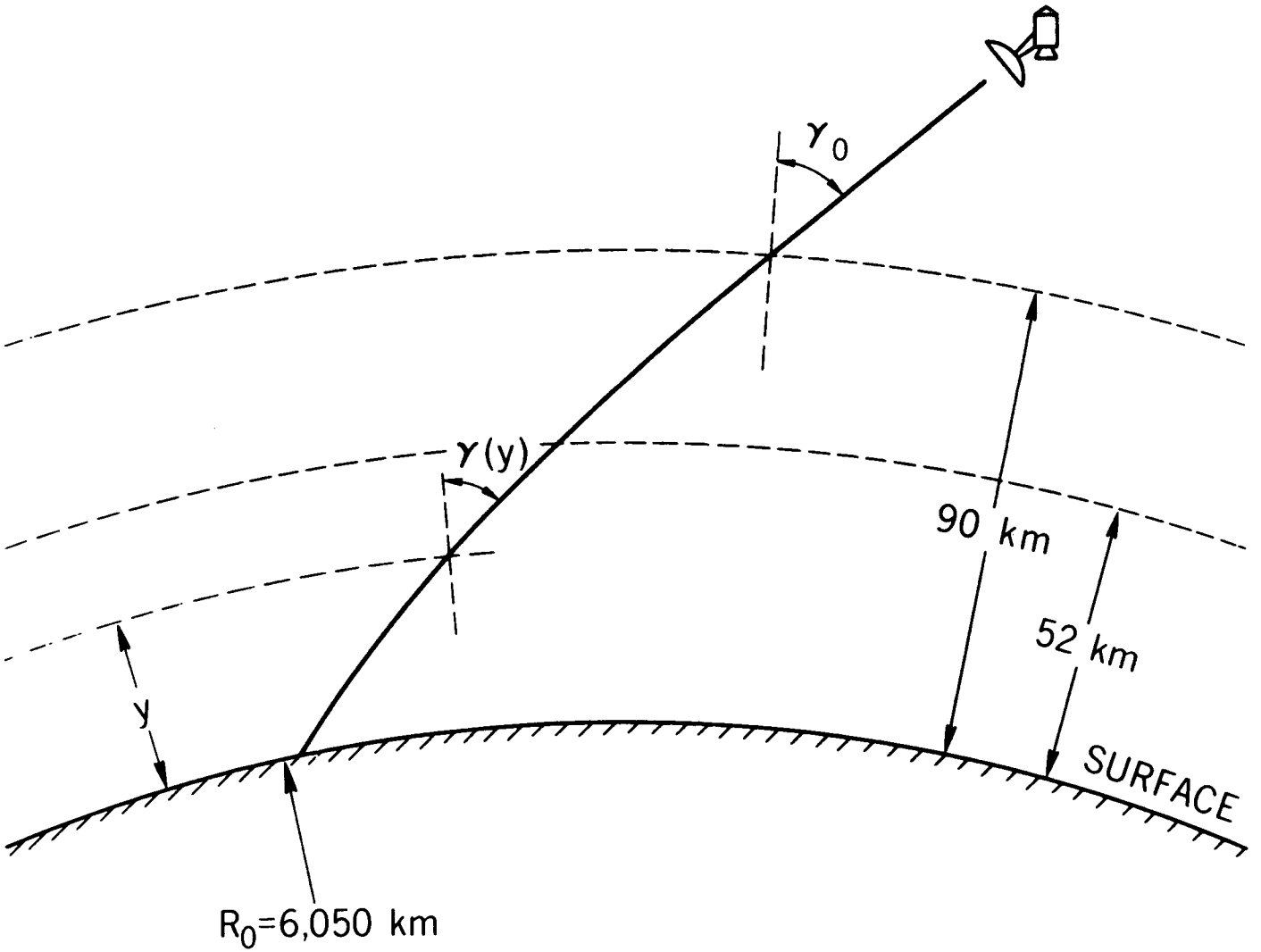

Figure 5. Spherical model of the atmospheric layers

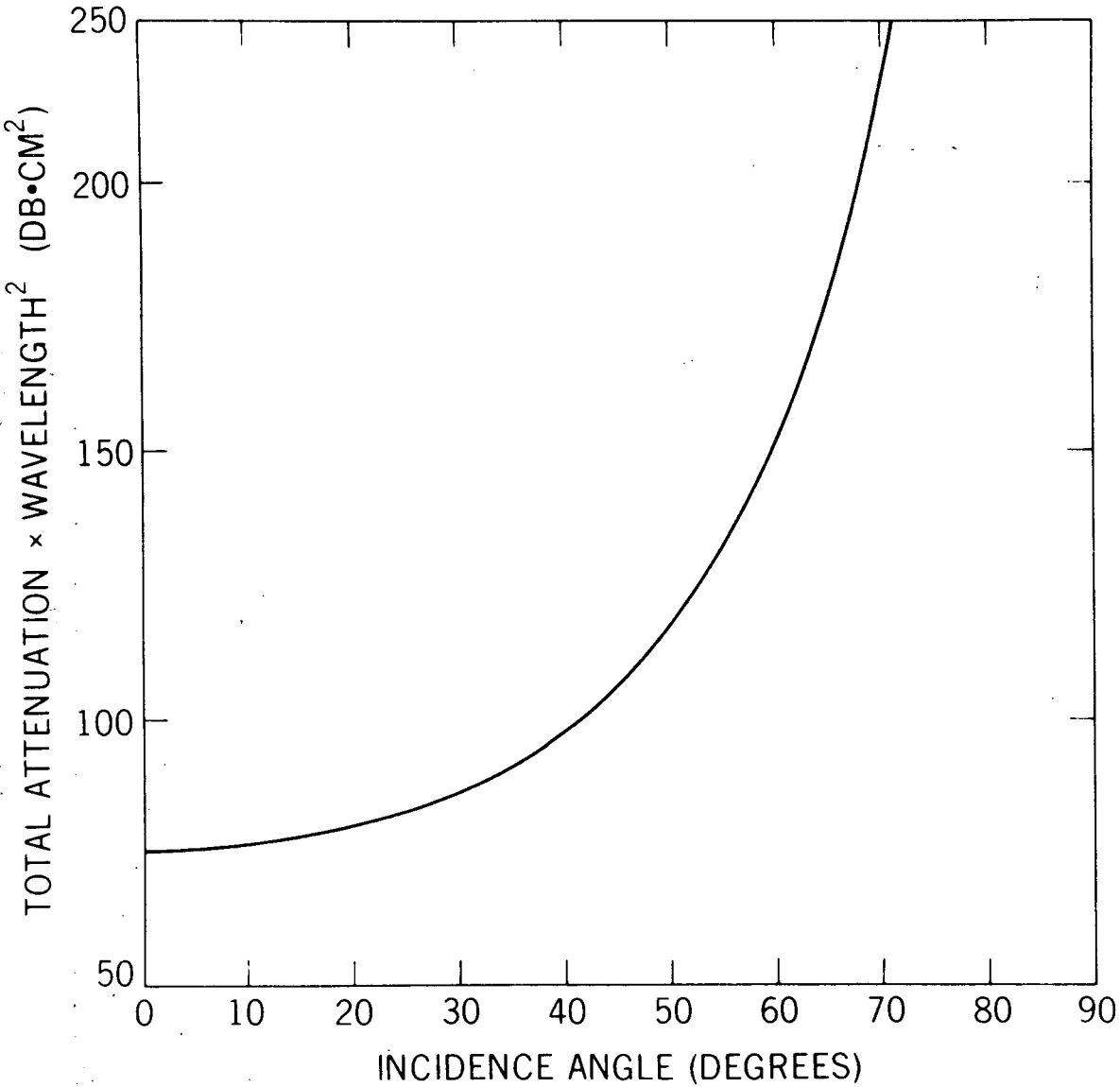

Figure 6. Normalized one-way attenuation vs incidence angle

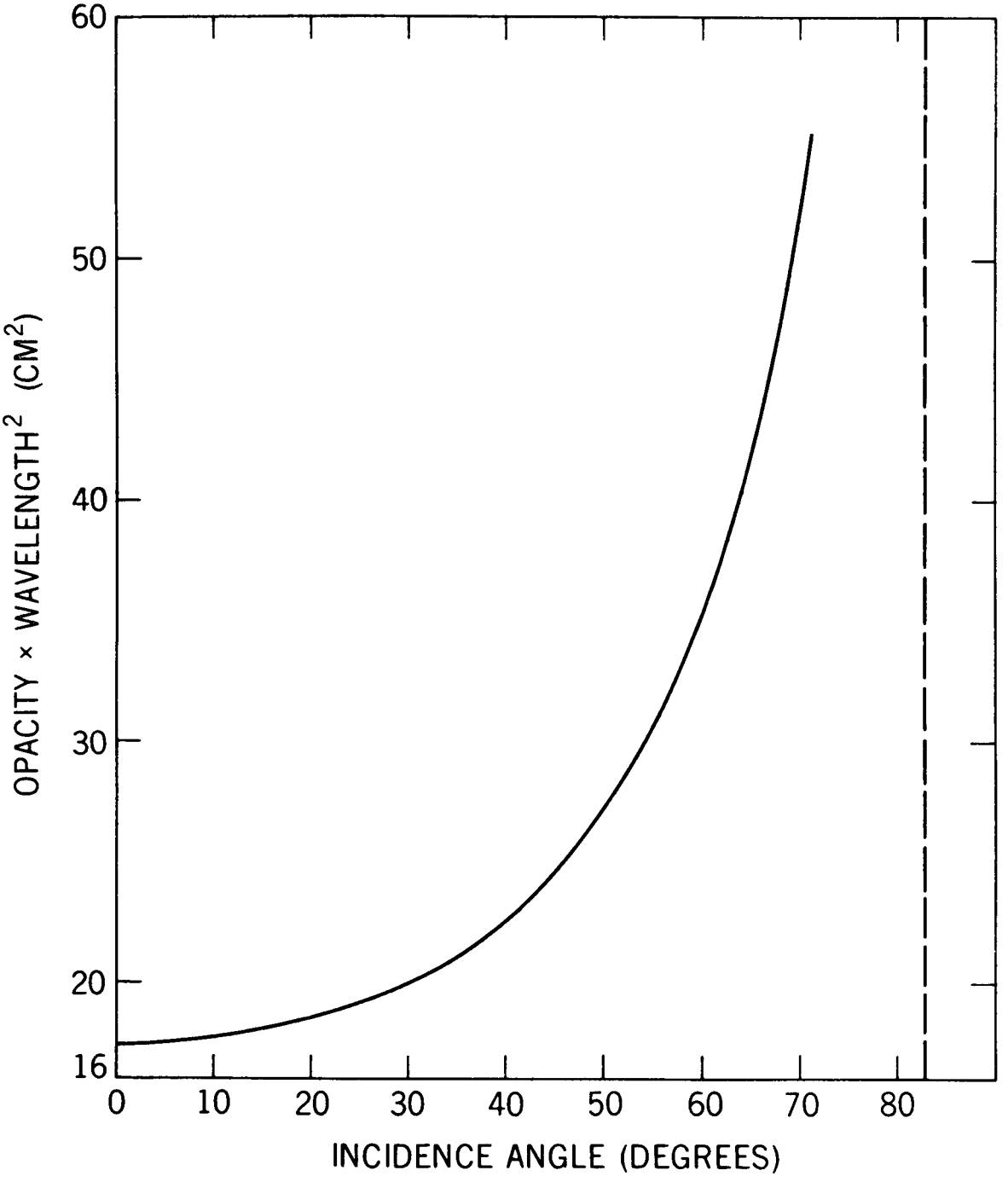

Figure 7. Normalized opacity vs. incidence angle

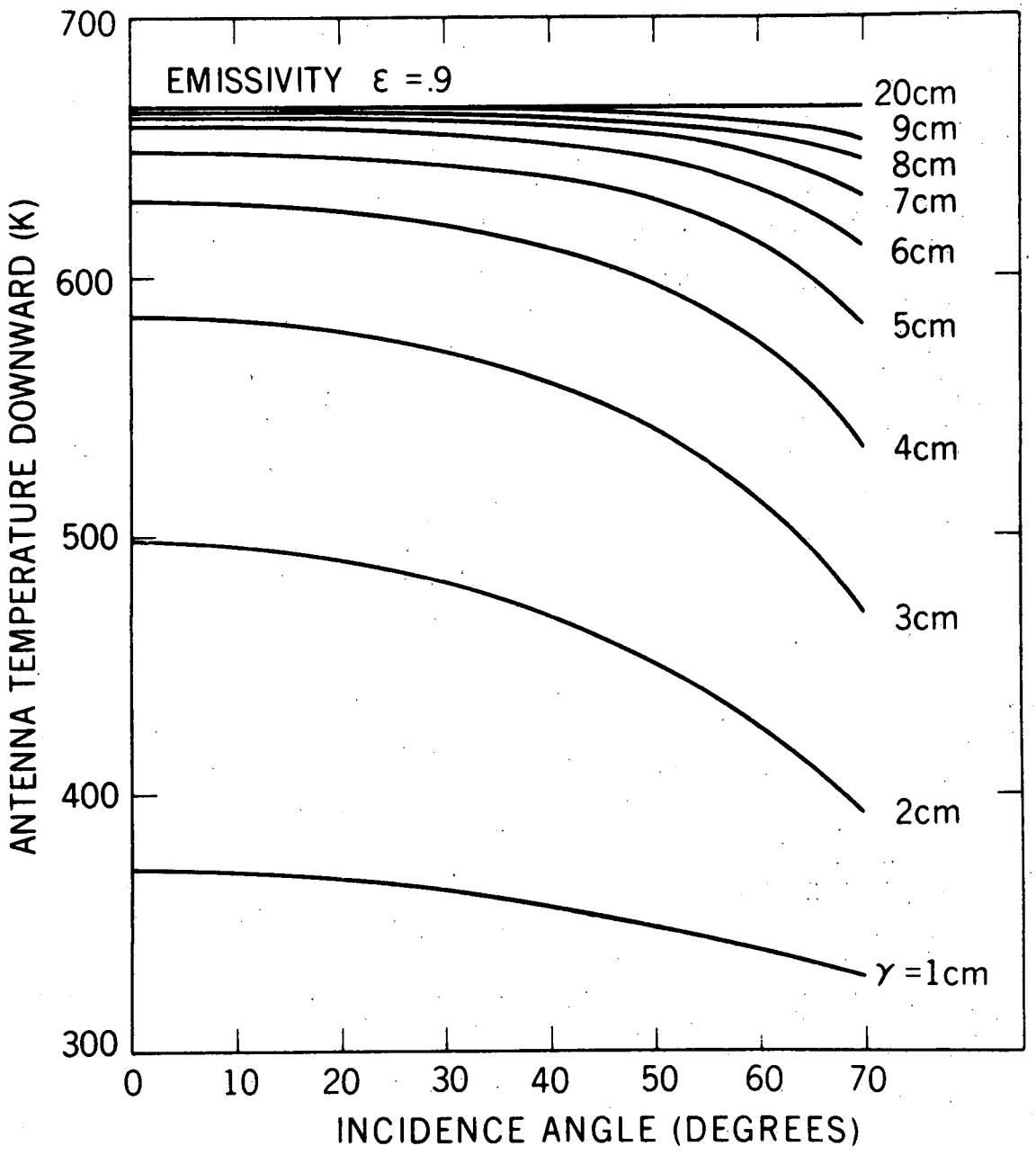

Figure 8. Antenna temperatures of a downward looking antenna

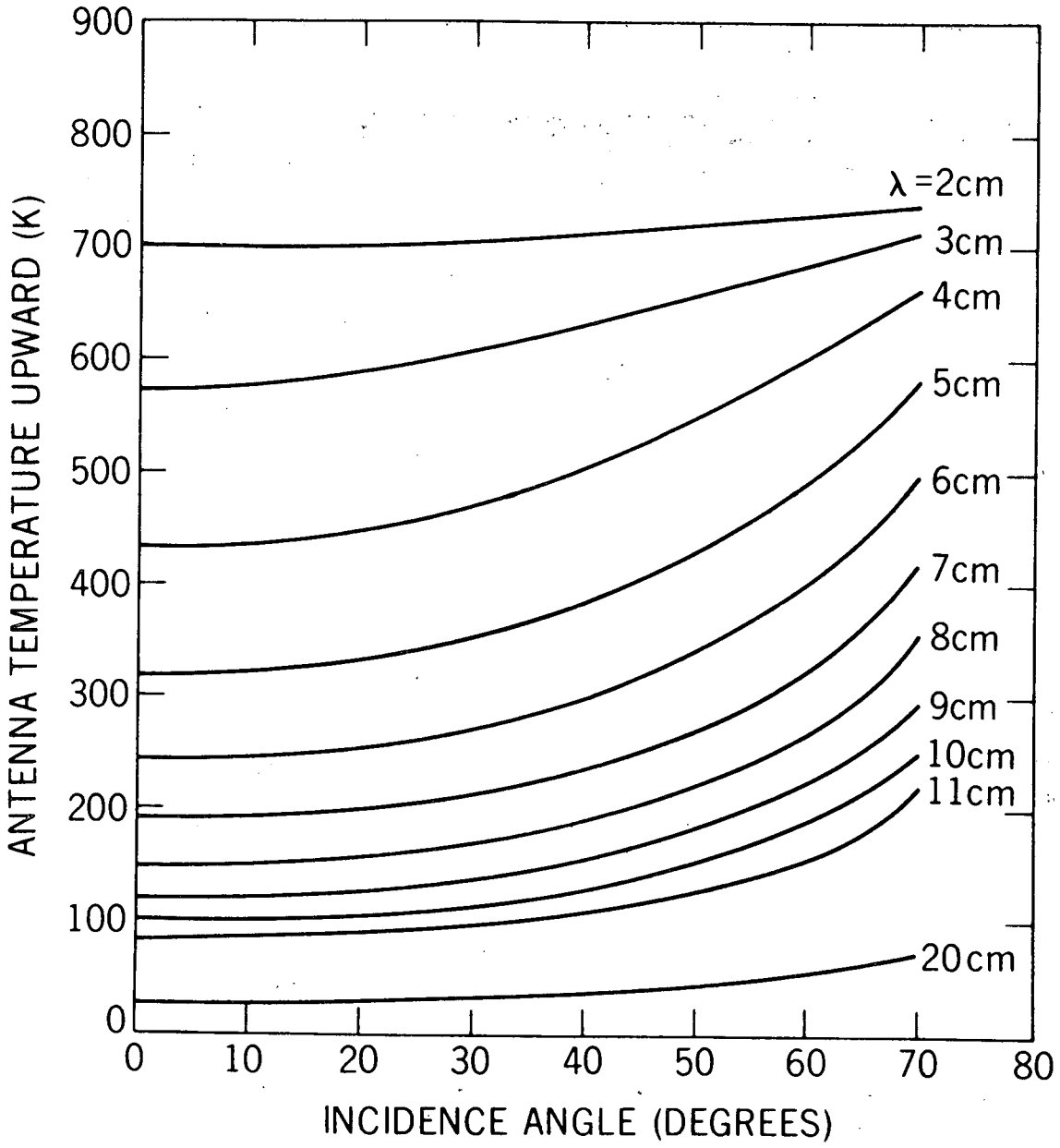

Figure 9. Antenna temperatures of an upward looking antenna

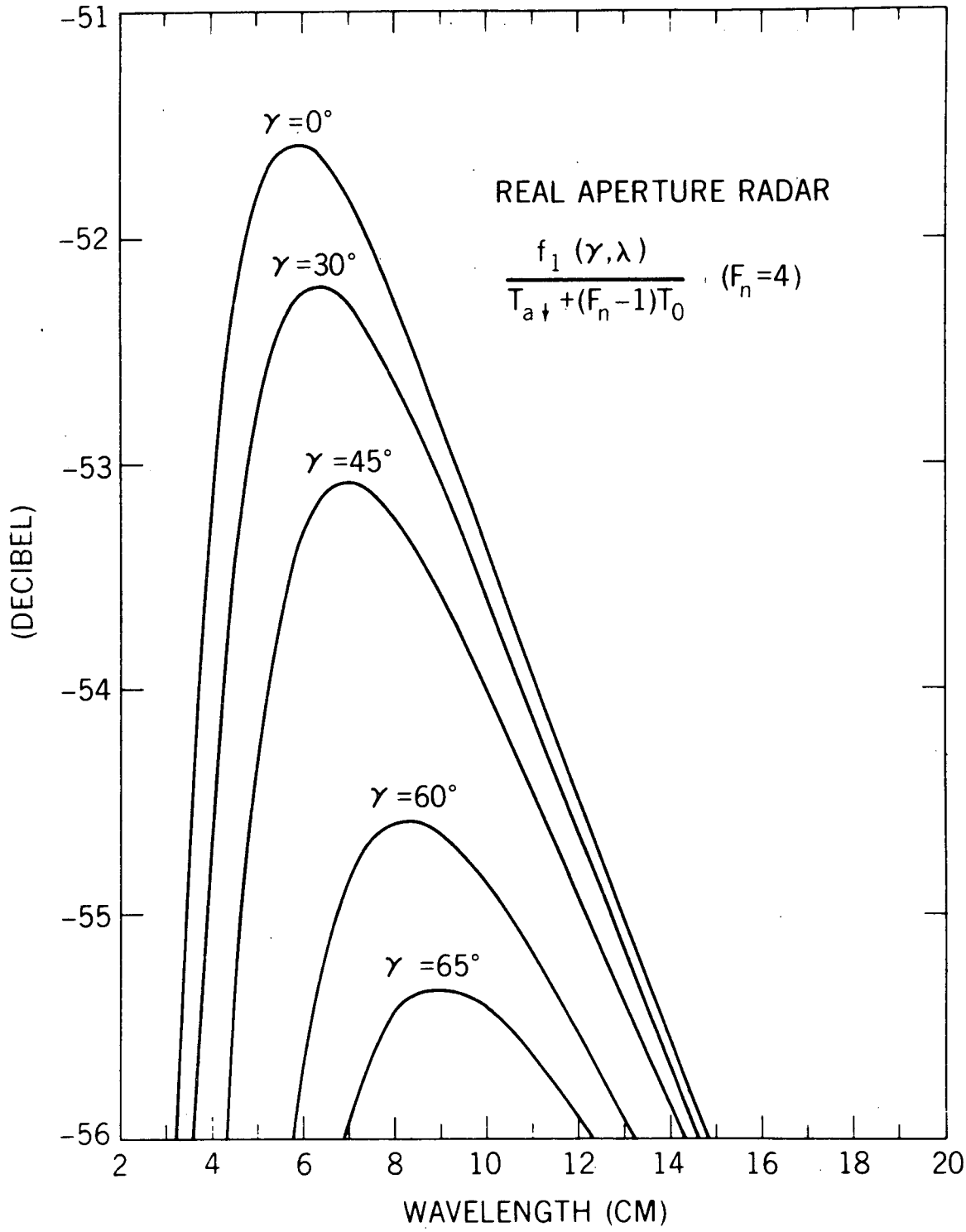

Figure 10. Wavelength depending term of the signal-to-noise ratio for a real aperture radar (RAR).

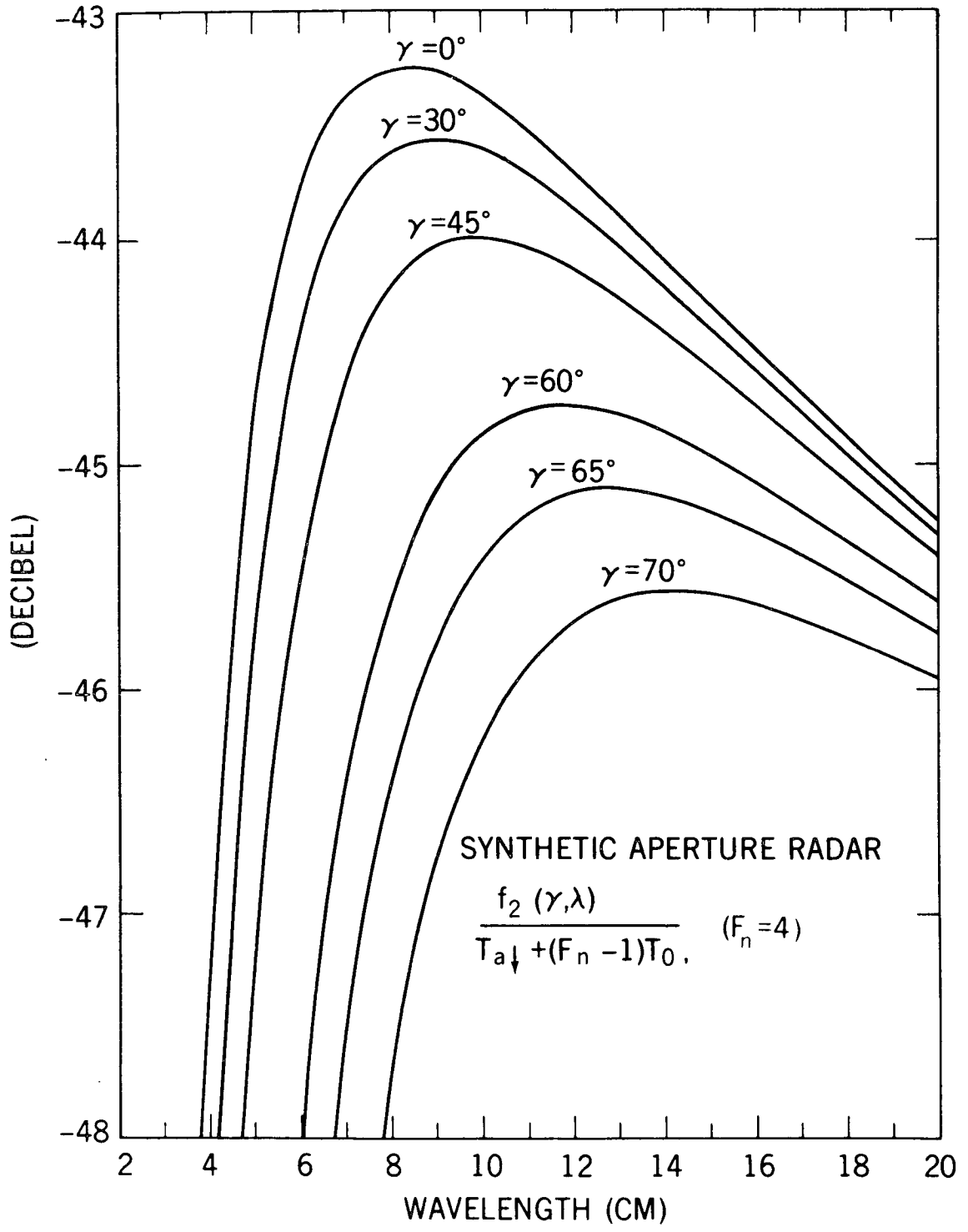

Figure 11. Wavelength depending term of the signal-to-noise ratio for a synthetic aperture radar (SAR)

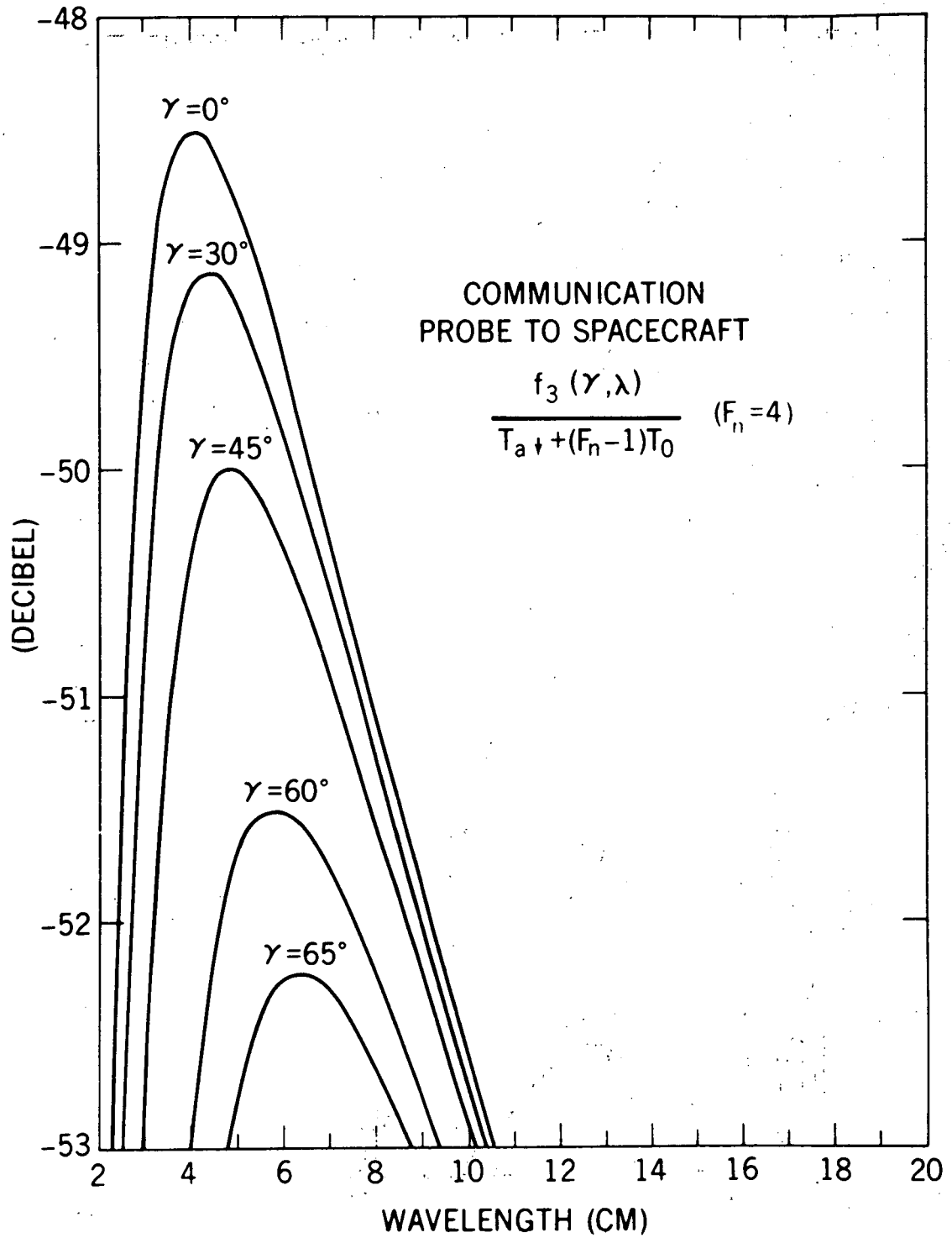

Figure 12. Wavelength depending term of the signal-to-noise ratio for an upward communication link (UL)

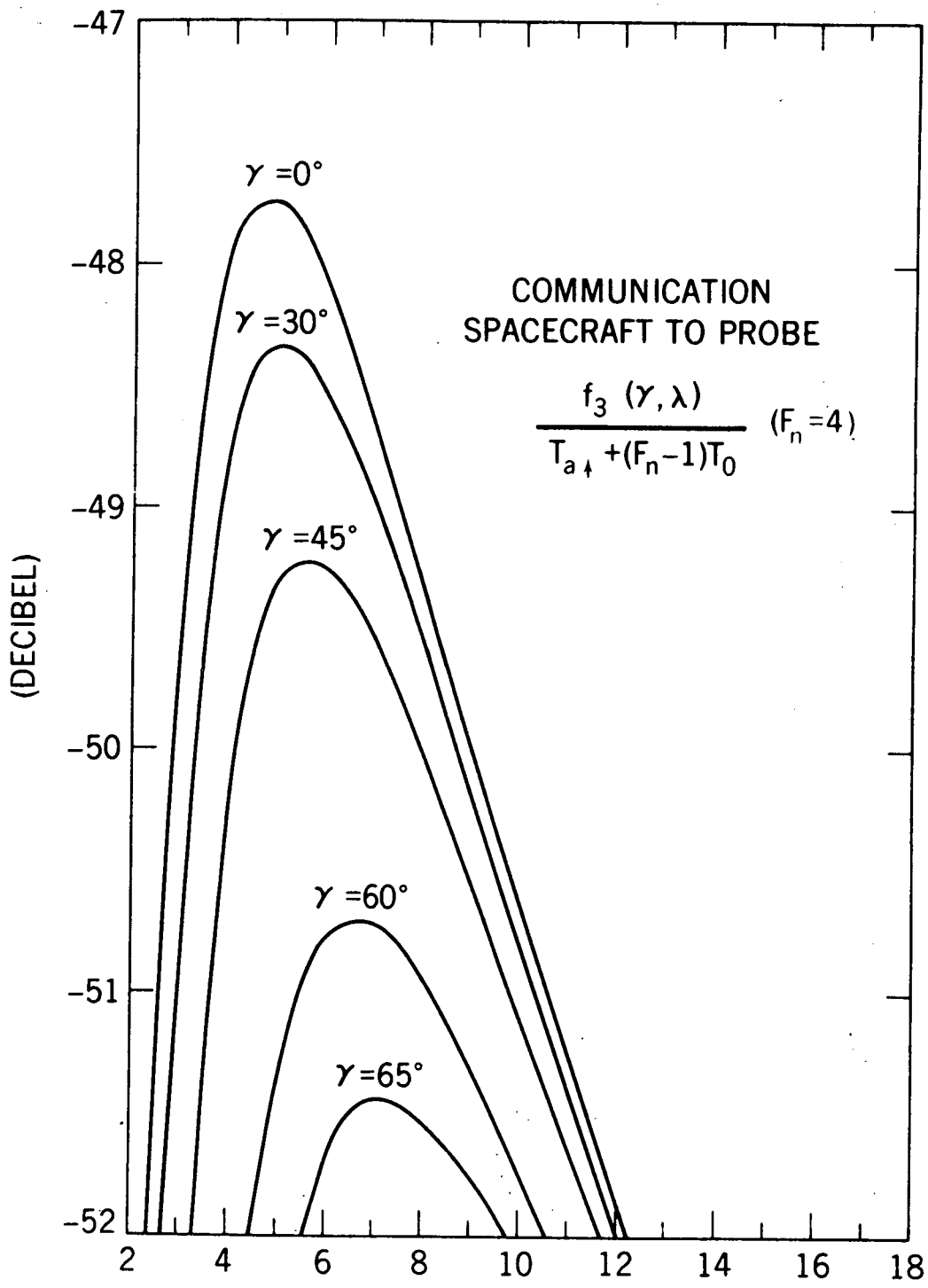

Figure 13. Wavelength depending term of the signal-to-noise ratio for a downward communication link (DL)

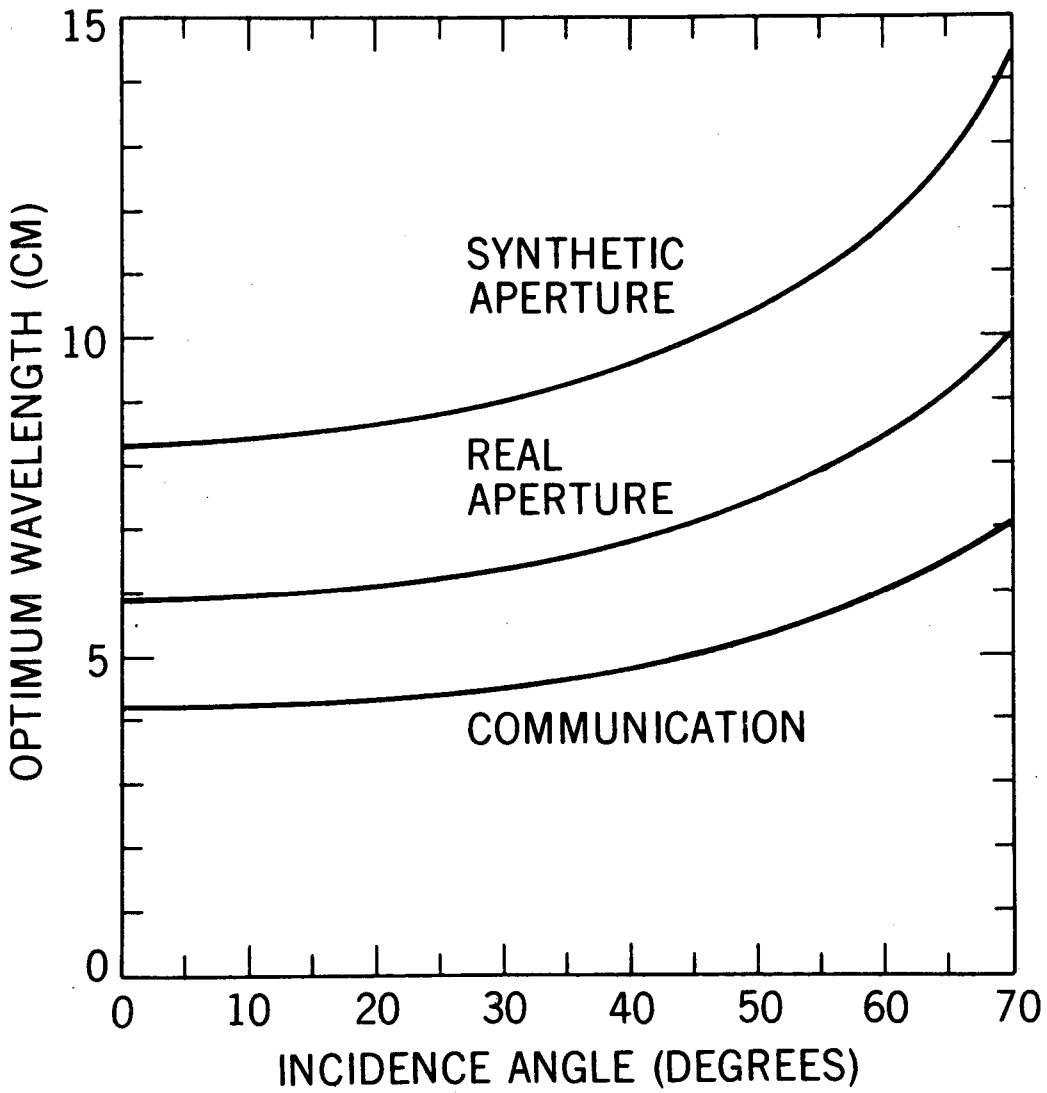

Figure 14. Optimum wavelengths versus incidence angle for RAR, SAR, and UL or DL

NASA–GSFC